

## Interaction of an outflow with surrounding gaseous clouds as the origin of the late-time radio flares in TDEs

JIALUN ZHUANG (庄嘉伦)<sup>1,2</sup> RONG-FENG SHEN (申荣锋)<sup>1,2</sup> GUOBIN MOU (牟国斌)<sup>3</sup> AND WENBIN LU (鲁文宾)<sup>4</sup>

<sup>1</sup>*School of Physics and Astronomy, Sun Yat-Sen University, Zhuhai, 519000, China*

<sup>2</sup>*CSST Science Center for the Guangdong-Hongkong-Macau Greater Bay Area, Sun Yat-Sen University, Zhuhai, 519082, China*

<sup>3</sup>*Department of Physics and Institute of Theoretical Physics, Nanjing Normal University, Nanjing 210023, China*

<sup>4</sup>*Department of Astronomy, University of California, Berkeley, CA 94720-3411, USA*

Submitted to ApJ

### ABSTRACT

Close encounter between a star and a supermassive black hole (SMBH) results in the tidal disruption of the star, known as a tidal disruption event (TDE). Recently, a few TDEs, e.g., ASASSN-15oi and AT2018hyz, have shown late-time (hundreds of days after their UV/optical peaks) radio flares with radio luminosities of  $10^{38\sim 39}$  erg/s. The super-Eddington fallback or accretion in a TDE may generate a mass outflow. Here we investigate a scenario that the late-time radio flares come from the interaction of the outflow with the circum-nuclear gaseous clouds, in addition to the slow-evolving emission component due to the outflow-diffuse medium interaction. We calculate the associated radio temporal and spectral signatures and find that they reproduce well the observations. The outflows have the inferred velocity of  $0.2 \sim 0.8 c$ , the total mass of  $10^{-3} \sim 10^{-1} M_{\odot}$  and the ejection duration of a month to a year. The distances of the clouds to the SMBH are  $0.1 \sim 1$  pc. This scenario has advantages in explaining the long delay, sharpness of the rise and the multiplicity of the late radio flares. Future observations may build up a much larger sample of late-time radio flares and enable their use as a probe of the TDE physics and the host circumnuclear environment.

*Keywords:* Tidal disruption event, late-time radio flares

### 1. INTRODUCTION

Most galaxies are considered to contain a supermassive black hole with a mass above  $\sim 10^6 M_{\odot}$  at its nuclei (Ferrarese & Ford 2005). A star wandering too close to the supermassive black hole would be tidally disrupted as a tidal disruption event (TDE) (Rees 1988; Phinney 1989). Accretion of the stellar debris would produce a bright flare in X-ray or UV/optical, which would last for months to years with the light curve decaying as  $t^{-\frac{5}{3}}$  (Rees 1988; Phinney 1989).

In TDEs, outflow can be produced via various mechanisms. At the moment of disruption, the unbound debris would fly away at a velocity of  $10^4$  km/s (Guillochon et al. 2016; Yalinewich et al. 2019). Besides, a fraction

of the matter initially bound to the black hole is likely to be blown away with a velocity of  $\sim 0.1c$ , where  $c$  is the light speed, by the radiation pressure when the fallback rate, or the accretion rate, of these bound debris is super-Eddington at early times (Strubbe & Quataert 2009; Bu et al. 2023b). Furthermore, for black holes with masses greater than  $10^7 M_{\odot}$ , the self-crossing of the fallback stream, due to relativistic apsidal precession, can also generate energetic, fast outflow, and the speed of these outflow ranges from  $\sim 0.01c$  to  $\sim 0.1c$  (Lu & Bonnerot 2020). Another possibility concerns the relativistic jet which can be generated in the presence of a large magnetic flux threading a rapidly spinning black hole (Blandford & Znajek 1977; Tchekhovskoy et al. 2011; Bloom et al. 2011; Burrows et al. 2011).

When the high-speed outflow or jet interact with the circumnuclear medium (CNM), it would drive a forward shock in the CNM, and produce radio emission via the synchrotron radiation (Chevalier 1998; Barniol Duran

E-mail: zhuangjlun@mail2.sysu.edu.cn (JZ); shenrf3@mail.sysu.edu.cn (RS); gbmou@njnu.edu.cn (GM); wenbinlu@berkeley.edu (WL)

et al. 2013). In the past decade, dozens of TDEs indeed have shown these GRB-afterglow-like radio emissions, and their radio luminosities span from  $10^{36}$  to  $10^{42}$  erg/s (Alexander et al. 2020). However, the most recent radio observations of some TDEs reveal flares only at a late time ( $10^2 \sim 10^3$  days after TDE discovery) which are difficult to be explained by the conventional outflow-CNM scenario due to the rapid evolution of light curves, such as ASASSN-15oi and AT2018hyz. The steepest evolution from the outflow-CNM interaction is  $f_\nu \propto t^3$  (Metzger et al. 2012; Krolik et al. 2016; Alexander et al. 2020), but ASASSN-15oi, as well as AT2018hyz, show a jump in flux density from non-detection to detection that requires a temporal power-law steeper than  $t^4$ .

Various models have been proposed to explain these late and steeply rising radio flares in TDEs. Cendes et al. (2023) conclude that the delayed outflows, such as from delayed disk formation, are a preferred explanation for these ubiquitous late radio emissions. However, a systematic analysis of the X-ray emission in optically selected TDEs that include those events showing late radio flares, by Guolo et al. (2023), favors the viewing-angle unification models instead of the delayed formation of the accretion disk because early X-ray detection indicates that the accretion disk responsible for the X-ray emission is already present at very early times. Likewise, early radio detection such as AT2019azh suggests that the outflow tends to be launched at the occurrence of TDEs.

In addition, Teboul & Metzger (2023) and Lu et al. (2023) propose a misaligned precessing jet, which is initially choked by the disk wind and may only break out later when the disk eventually aligns itself with the BH spin axis due to the viscous damping of the precession. This jet may produce delayed radio rebrightening seen in TDEs. An alternative model is that of a decelerated off-axis jet (Matsumoto & Piran 2023; Sfaradi et al. 2024), which we will address in Section 5. Besides, Matsumoto & Piran (2024) find that a power-law CNM density profile followed by a constant outside the Bondi radius can explain the radio flares in AT2020vwl, AT2019dsg, PS16dtm and ASASSN14ae, though it is difficult to explain a rise steeper than  $\propto t^3$  like in AT2018hyz.

In the active galactic nuclei, the SMBH is thought to be surrounded by a torus composed of gas clumps or clouds (Krolik & Begelman 1988; Antonucci 1993). It is natural to suspect there are circum-nuclear clouds in non-active galaxies as well. One direct evidence comes from the observation of the Milky Way galactic center, which reveals that there are clouds near the Sgr  $A^*$ , and the distribution of these clouds indicates a ring-like structure (Mezger et al. 1996; Christopher et al. 2005).

Mou et al. (2022) propose the outflow–cloud interaction can generate considerable radio emission, which may account for the radio flares appearing months or years later after TDE outbursts, and successfully explain the temporal evolution of the peak frequencies of AT2019dsg (Cendes et al. 2021), ASASSN-14li (Alexander et al. 2016), and CSS161010 (Coppejans et al. 2020). Based on the TDEs wind-cloud interaction model, Bu et al. (2023a) find that the predicted peak radio emission frequency, the luminosity at peak frequency, and their time evolution can be well consistent with those in TDEs AT2019dsg (Cendes et al. 2021) and ASASSN-14li (Alexander et al. 2016). Besides the delayed radio flares, outflow-cloud interaction could also produce some other kinds of afterglows, such as neutrinos (Mou & Wang 2021; Wu et al. 2022), gamma-rays (Mou & Wang 2021), and X-rays (Mou et al. 2021; Chen & Wang 2023).

Here, we investigate the outflow-cloud interaction model for these late-time radio flares, where the outflow mass loss rate follows a power law decay with time. This collision forms a bow shock in front of the inner face of the cloud, across which electrons are accelerated and the magnetic field is amplified. The late-time radio synchrotron emission is expected from the shocked outflow. An illustration of the interaction of the TDE outflow with the cloud is shown in Figure 1.

In section 2, we introduce the semi-analytical model for the wind-cloud interaction and calculate the associated synchrotron emission. We also take into account the effect of the interaction of the outflow with a diffuse CNM in section 3. The application of our model to a few TDEs will be presented in section 4. Discussion and conclusion will be given in sections 5 and 6, respectively.

## 2. INTERACTION OF THE OUTFLOW WITH THE CLOUD

### 2.1. The clouds

Radio observations revealed tens of molecular clouds at a distance of  $0.5 \sim 2$  pc from Sgr  $A^*$  (Mezger et al. 1996; Christopher et al. 2005). The typical mass of a cloud is  $10^4 M_\odot$  with a gas number density of  $10^6 \sim 10^8 \text{ cm}^{-3}$  and a size of about 0.1 pc, and the total mass of the torus is about  $10^6 M_\odot$  (Mezger et al. 1996; Christopher et al. 2005). As for AGN, the clouds near the black hole have a smaller size of  $10^{13 \sim 14}$  with a higher density of  $10^{8 \sim 12} \text{ cm}^{-3}$  at a similar distance of  $10^{16 \sim 17} \text{ cm}$  (Armijos-Abendaño et al. 2022). Here we consider the simplest case where the outflow interacts with a cloud at a distance  $R_{in} \approx 0.1 \sim 1$  pc to the central blackhole and of a radius  $R_c \approx 0.01 \sim 0.1$  pc.

### 2.2. The outflow

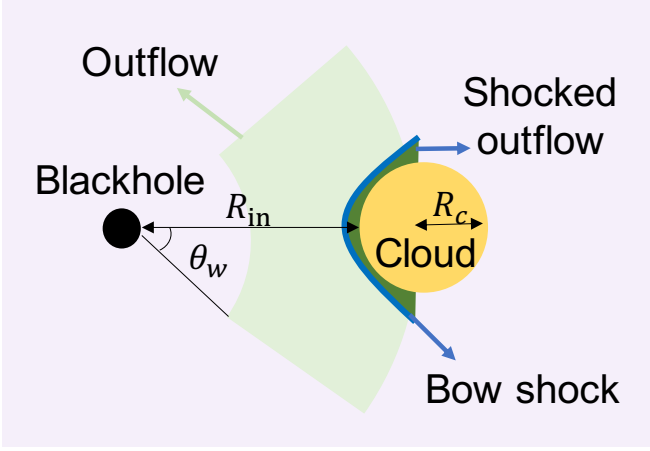


**Figure 1.** Schematic of the interaction of the TDE outflow with the cloud. Outflow is generated at the occurrence of TDEs near the black hole with a half opening angle  $\theta_w$  and a velocity  $v_w$ . The cloud is located at a distance of  $R_{in}$  with a radius  $R_c$ . The interaction of the outflow with the cloud leads to the formation of a bow shock, producing a late-time radio flare years after TDE. This illustration is not to scale.

We assume that an accretion-driven outflow was launched at the time of the TDE ( $t = 0$ ). For simplicity, we take its shape to be conical, with a half opening angle of  $\theta_w = \pi/4$  (a solid angle of  $\Omega_w \sim 2$ , [Curd & Narayan \(2019\)](#)). The outflow has a mean velocity of  $v_w$ , and the velocities of its front and rear ends are  $v_w \pm av_w$ , respectively. The velocity spread is  $a \approx 0.1 \sim 0.6$  according to the super-Eddington accretion simulation of TDEs ([Dai et al. 2018](#); [Bu et al. 2023b](#)). Hereafter we set  $a=0.1$  in all the calculation. The effect of a larger  $a$  will be discussed at the end of Section 2.4.

The outflow was launched for a duration of  $t_w \sim$  months. Due to the velocity spread, the radial width of the outflow grows as  $\Delta(r) \approx 2ar + \Delta_0$ , where  $\Delta_0 = v_w t_w$  and  $r = v_w t$ .

We define  $t'$  as the elapsed time since the start of the outflow-cloud collision, then the temporal evolution of the outflow mass rate  $\dot{m}(t', r)$  at distance  $r$  will determine the outflow's density during the collision. We assume it increases linearly over time with a peak at  $t' = t_w(r) \equiv t_w \Delta(r)/\Delta_0$  and then follows a power law decay:

$$\dot{m}_w(t', r) = \frac{\dot{m}_0 \Delta_0}{\Delta(r)} \times \begin{cases} \frac{t'}{t_w(r)}, & t' < t_w(r), \\ \left[ \frac{t'}{t_w(r)} \right]^{-5/3}, & t_w(r) \leq t', \end{cases} \quad (1)$$

where  $\dot{m}_0$  is the peak mass loss rate near the SMBH and then the total mass of the outflow is  $m_w = \int \dot{m}_w(t', r) dt$ .

### 2.3. Radiation properties

Assuming a fraction  $\epsilon_b$  of the pre-shock outflow kinetic energy is converted into the magnetic energy density  $B^2/(8\pi) = \epsilon_b \rho_w v_w^2$  ([Sari et al. 1998](#); [Yalinewich et al. 2019](#)), the magnetic field strength can be obtained as:

$$B = \sqrt{8\pi \epsilon_b \rho_w v_w} \\ \approx 0.1 \Omega_w^{-\frac{1}{2}} \epsilon_{b,-3}^{\frac{1}{2}} \dot{m}_{w,-1}^{\frac{1}{2}}(t', r) \beta_{w,-1}^{\frac{1}{2}} R_{in,-1}^{-1} \text{ [G]} \quad (2)$$

where  $\epsilon_{b,-3} \equiv \epsilon_b/0.001$ ,  $\dot{m}_{w,-1}(t', r) \equiv \dot{m}_w(t', r)/(0.1 \text{ M}_\odot/\text{yr})$ , and  $R_{in,-1} \equiv R_{in}/0.1 \text{ pc}$ . Here  $\epsilon_b$  has a wide range from  $10^{-4}$  to  $10^{-1}$  ([Granot & van der Horst 2014](#); [Santana et al. 2014](#); [Zhang et al. 2015](#); [Beniamini et al. 2016](#)).

The synchrotron radiation power and characteristic frequency from an electron with a Lorentz factor of  $\gamma_e$  are  $P(\gamma_e) = \sigma_t c \gamma_e^2 B^2/(6\pi)$  and  $\nu(\gamma_e) = q_e B \gamma_e^2/(2\pi m_e c)$ , respectively, then the peak spectral power is  $P_{\nu,max} = P(\gamma_e)/\nu(\gamma_e) = m_e c^2 \sigma_t B/(3q_e)$  and is independent of  $\gamma_e$  ([Sari et al. 1998](#)). Thus, the synchrotron peak flux density of the swept-up electrons is  $F_{\nu,max} = N_e P_{\nu,max}/(4\pi D^2)$ , where  $D$  is the distance of the source and  $N_e$  is the total number of emitting electrons.

#### 2.3.1. Time dependence of Radiating electrons

The number of emitting electrons at any given time  $t'$  is:

$$N_e(t') = \frac{\Omega_c \int_0^{t'} \dot{m}_w(t', r) dt}{\Omega_w m_p}, \quad (3)$$

where  $\Omega_c$  is the solid angle of the cloud with respect to the SMBH, so  $\Omega_c/\Omega_w < 1$  is the fraction of the outflow that indeed interacts with the cloud.

However, these electrons would cool due to both radiation and expansion ([Dai et al. 1999](#)), which needs to be taken into account in Eq.(3). The synchrotron cooling time for electrons with  $\gamma_e$  is ([Sari et al. 1998](#))

$$t_{syn} = \frac{6\pi m_e c}{\sigma_t \gamma_e B^2} \\ = 7.7 \times 10^{10} \gamma_e^{-1} B_{-1}^{-2} \text{ [s]}. \quad (4)$$

The adiabatic cooling timescale  $t_{ad}$  is generally estimated as the time required for the flow to cross the characteristic spatial scale  $t_{dyn} \equiv R_c/v_w \approx 10^7 R_{c,-2} \beta_{w,-1} \text{ s}$  where  $R_{c,-2} \equiv R_c/0.01 \text{ pc}$  ([Barkov et al. 2019](#)). However, according to the simulation of outflow-cloud interaction in [Mou & Wang \(2021\)](#), in the case of a long-lasting outflow  $t_w \gg t_{dyn}$ , the motion of the post-shock stream is confined by the shocked outflow rather than being a free expansion, while it approaches the free expansion if  $t_w \leq t_{dyn}$ . Therefore, we use the following

fitting formula (see Figure B2 in Mou & Wang. 2021) to estimate  $t_{ad}$

$$t_{ad} = \begin{cases} t_{dyn}, & (t_w/t_{dyn}) \leq 1, \\ 1.36t_w - 0.36t_{dyn}, & 1 < (t_w/t_{dyn}) < 15, \\ 20t_{dyn}, & 15 \leq (t_w/t_{dyn}). \end{cases} \quad (5)$$

The Lorentz factor of electrons which radiate mainly in GHz is about  $\gamma_e \sim 50$  since  $B$  is of the order of 0.1 G, and we have  $t_{syn} \approx 10^9$  s  $\gg t_{ad}$ . Therefore, the electron cooling is dominated by the adiabatic expansion.

Taking this cooling timescale into account, Eq.(3) would be corrected as:

$$N_e(t') = \frac{\Omega_c \int_{t'-t_{ad}}^{t'} \dot{m}_w(t', r) dt}{\Omega_w m_p}, \quad (6)$$

since the electrons accelerated at a time of  $t_{ad}$  earlier would have all cooled down.

### 2.3.2. Synchrotron spectrum

The synchrotron flux density at any given frequency can be calculated with  $F_{\nu, max}$  and the spectral shape (Sari et al. 1998). Electrons are usually accelerated to a power-law distribution as  $dN(\gamma_e) = C\gamma_e^{-p}d\gamma_e$ ,  $\gamma_e > \gamma_m$  where  $p = 2.5$  is the spectral index and  $\gamma_m$  is the minimum Lorentz factor of the electrons (Sturmer et al. 1997; Gaisser et al. 1998; Sari et al. 1998). The coefficient  $C = (p-1)\gamma_m^{p-1}N_e(t')$  is obtained with  $\int_{\gamma_m}^{\infty} dN(\gamma_e) = N_e(t')$ . Assuming a fraction  $\epsilon_e$  of the outflow's kinetic energy goes into accelerating electrons,  $\gamma_m$  can be calculated based on the total energy of the accelerated electrons:  $\gamma_m = \frac{1}{2}\epsilon_e(m_p/m_e)[(p-2)/(p-1)]\beta_w^2$ .

The spectrum produced by these power-law electrons is featured with three breaking frequencies. Figure 2 shows all the six possible spectra cases, each of which consists of three or four power law segments, and the red star marks  $F_{\nu, max}$  (Granot & Sari 2002; Gao et al. 2013).

The first breaking frequency is the characteristic frequency:

$$\nu_m = \frac{\gamma_m^2 e B}{2\pi m_e c} \approx 1 \times 10^6 B_{-1} \gamma_{m,2}^2 \text{ [Hz]}, \quad (7)$$

where  $\gamma_{m,2} \equiv \gamma_m/2$ .

The second is the self-absorption frequency  $\nu_a$ , below which the emitting region is optically thick. It can be obtained by solving  $\int \alpha_\nu dl \approx \alpha_\nu l = 1$  where  $l$  is the radial width of the emitting region and  $\alpha_\nu \sim 10^{13}(C/\Omega_c R_{in}^2)B^{(p+2)/2}\nu^{-(p+4)/2}$  is the self-absorption

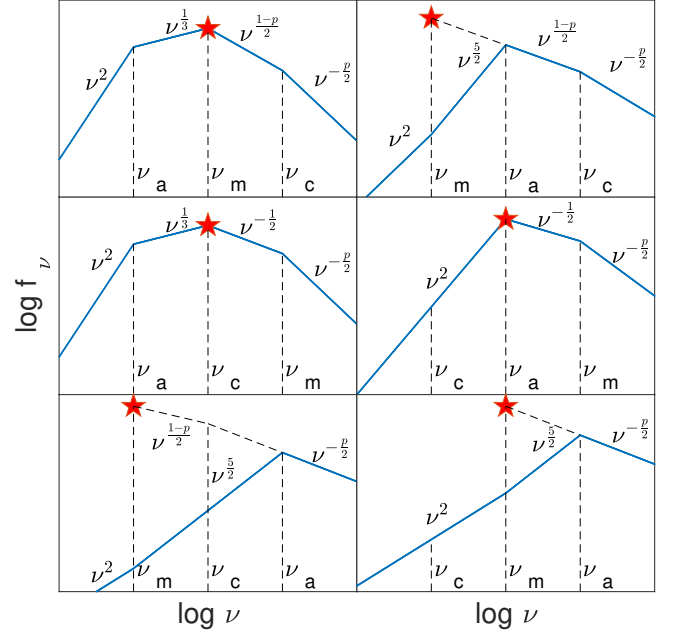


**Figure 2.** The possible synchrotron spectra from the shocked electrons. The spectral shape is determined by the relative ordering of the self-absorption frequency  $\nu_a$ , the characteristic frequency  $\nu_m$ , and the cooling frequency  $\nu_c$ . The red star marks  $F_{\nu, max}$ .

coefficient (Rybicki & Lightman 1986). Thus, this frequency is numerically estimated as:

$$\nu_a \approx 5.4 \times 10^9 \Omega_w^{-\frac{p+6}{2(p+4)}} \epsilon_e^{\frac{2}{p+4}} \epsilon_{b,-1}^{\frac{p+2}{2(p+4)}} \gamma_{m,2}^{\frac{2(p-2)}{p+4}} \dot{m}_{w,-1}^{\frac{p+6}{2(p+4)}} \beta_{w,-1}^{\frac{p+10}{2(p+4)}} R_{in,-1}^{-\frac{p+6}{p+4}} t_2^{\frac{2}{p+4}} \text{ [Hz]}. \quad (8)$$

where  $t_2' \equiv t'/100$  days.

The cooling frequency  $\nu_c$ , where electrons with Lorentz factor  $\gamma_c$  would have cooled down in the time  $t'$ , can be obtained by solving  $\gamma_c m_e c^2 = P(\gamma_c)t'$  which gives  $\gamma_c = 6\pi m_e c/(\sigma_t B^2 t')$  (Sari et al. 1998), and the corresponding cooling frequency is

$$\nu_c = 1.6 \times 10^{13} B_{-1}^3 t_2'^{-2} \text{ [Hz]}. \quad (9)$$

A comparison of these three breaking frequencies suggests that the upper right case ( $\nu_m < \nu_a < \nu_c$ ) in Figure 2 is concerned most of the time. Given that the observational frequencies are near the peak frequency which would lead to significant deviation in flux by our asymptotic computation, here we smooth our analytical spectra with the following equation (Granot & Sari 2002):

$$F_\nu = F_\nu(\nu_m) \left[ \left( \frac{\nu}{\nu_m} \right)^2 \exp(-s_4(\nu/\nu_m)^{2/3}) + \left( \frac{\nu}{\nu_m} \right)^{5/2} \right] \times \left[ 1 + \left( \frac{\nu}{\nu_a} \right)^{s_5(\beta_2 - \beta_3)} \right]^{-1/s_5}, \quad (10)$$

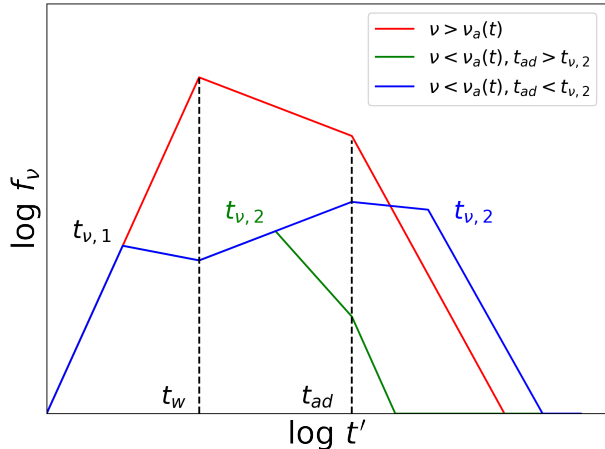


**Figure 3.** Sketch of the predicted radio light curve from the interaction of the outflow with the cloud at different frequencies. The red line represents the light curve for frequencies that always have  $\nu > \nu_a(t')$  while the green and blue lines are for the cases in which  $\nu_a$  crosses  $\nu$  at times  $t_{\nu,1}$  and  $t_{\nu,2}$ , respectively. Note that the horizontal axis  $t'$  is the time since the start of the collision.

where  $\beta_2 = 5/2, \beta_3 = (1-p)/2, s_4 = 3.63p - 1.6$  and  $s_5 = 1.25 - 0.18p$ .

#### 2.4. Light curve from the shocked outflow

The radio flare from the outflow-cloud interaction would appear at a time of  $R_{in}/v_w \sim 0.1 \text{ pc}/0.1 \text{ c} \sim 10^8 \text{ s}$  (years after TDEs). The peak luminosity at 1 GHz at time  $t' = t_w(r)$  can be crudely estimated as:

$$\begin{aligned} \nu L_\nu &= \nu_a N_e P_{\nu, \max} \left( \frac{\nu_a}{\nu_m} \right)^{\frac{1-p}{2}} \\ &\approx 8 \times 10^{38} \Omega_c \Omega_w^{-\frac{19+3p}{2(p+4)}} \epsilon_{e,-1} \epsilon_{b,-3}^{\frac{3p+5}{2(p+4)}} \\ &\gamma_{m,2}^{\frac{4p-11}{p+4}} \dot{m}_{0,-1}^{\frac{3p+19}{2(p+4)}} \beta_{w,-1}^{\frac{7p+21}{2(p+4)}} R_{in,-1}^{-\frac{2p+22}{2(p+4)}} t_2^{\frac{7}{p+4}} \text{ [erg/s]}. \end{aligned} \quad (11)$$

Since  $\nu_a$  changes with the density of the outflow and peaks at  $t_w$ , the flux at different frequencies would evolve differently. Figure 3 shows the sketch of the predicted radio light curve at different frequencies.

For  $\nu > \nu_a(t')$  (red line), the radio light curve would vary with the growth of the density of the outflow as  $F_\nu = F_{\nu, \max} (\nu/\nu_m)^{(1-p)/2} \propto t'^{(p+9)/4}$ . Later it would peak at  $t_w(r)$ , when the density of the outflow starts declining in the power-law form while  $N_e(t')$  remains nearly unchanged. As  $t'$  passes  $t_{ad}$ , the decrease in  $N_e(t')$  due to the adiabatic expansion would make  $f_\nu$  decrease more rapidly.

For  $\nu < \nu_a(t')$  (green line), as  $\nu_a$  increases with time, the light curve would decline as  $F_\nu = F_{\nu, \max} (\nu/\nu_m)^{(1-p)/2} (\nu/\nu_a)^{(p+4)/2} \propto t'^{-1/4}$  after  $t_{\nu,1}$ . Later when  $\nu_a$  peaks at  $t_w$  and starts to decrease, the

light curve would rise again as  $F_\nu \propto t'^{13/12}$  and then decline as  $F_\nu \propto t'^{-5(p+1)/12}$  once  $\nu_a$  drops below  $\nu$ . Likewise, the light curve would decrease faster after  $t_{ad}$ .

It is worth noting that the decrease in  $N_e(t')$  would start earlier than  $t_{\nu,2}$  (blue line). In this case, the radio light curve would peak at  $t_{ad}$ , and its subsequent decay would be slowed (or even re-rise) as  $\nu_a$  drops to  $\nu$ . Later when  $\nu_a$  crosses  $\nu$ , the light curve would decline faster.

It is clear from the above discussion that the light curve of the radio flare would rise on the timescale of  $t_w(r)$ , which is in turn determined by the width of the outflow  $\Delta(r)$ . Since usually  $t_w(r) \ll t$  for  $a \ll 1$ , it would be natural for this model to reproduce the observed sharp rise of the late radio flare.

However, a larger  $a$  would cause a wider width, and thus a shallower rise of the light curve. We found that a small velocity spread is required in order to match the data, therefore  $a = 0.1$  is set in this paper.

### 3. THE OUTFLOW-CNM INTERACTION

Besides the clouds, there is almost certainly a diffuse CNM and the interaction of outflow with the CNM would produce radio emission as well. Furthermore, changes in the velocity of the outflow due to its interaction with the CNM would affect the radiation properties from the bow shock.

Here we assume a CNM density profile  $n_{CNM}(r) = Ar_{-2}^{-1} \text{ cm}^{-3}$  where  $A$  is a constant and  $r_{-2} \equiv r/10^{-2} \text{ pc}$ , similar to the density distribution of CNM around Sgr A\* (Xu et al. 2006; Gillessen et al. 2019). We model the hydrodynamic evolution of the outflow under a set of hydrodynamical equations (Huang et al. 2000) :

$$\frac{dr}{dt} = \beta_w c \quad (12)$$

$$\frac{dM}{dr} = \Omega_w r^2 n_{CNM} m_p, \quad (13)$$

$$\frac{d\beta_w}{dM} = -\frac{\beta_w(1 + \beta_w^2/4)}{m_w + M + (1 - \epsilon)(1 + \beta^2)M}, \quad (14)$$

where  $M$  is the swept mass of the CNM by the forward shock and  $\epsilon$  describes the radiation efficiency.

Integrating these equations with proper initial conditions, we can obtain the hydrodynamic evolution of the outflow, and calculate the associated radiation properties from the shocked CNM according to Sari et al. (1998).

We then investigate the parameters dependence of the radio light curve from the shocked CNM. Figure 4 shows the predicted radio light curves at different CNM density values and profiles. The radio light curve would rise until it reaches the peak at  $t_{dec}$  after which the forward shock starts to decelerate. The deceleration timescale  $t_{dec}$  can

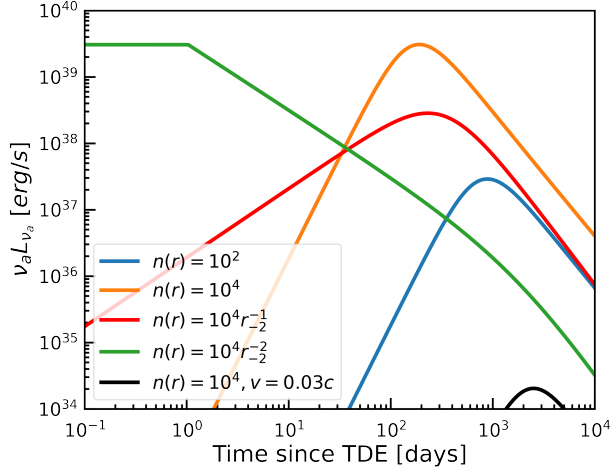


**Figure 4.** Predicted radio light curves from the interaction of the outflow with CNM. The density distributions of the CNM are shown in the legend. Other parameters as  $\epsilon_e = 0.01$ ,  $\epsilon_b = 0.001$ ,  $m_w = 0.1 M_\odot$  and  $v_w = 0.3c$ , or otherwise specified.

be crudely estimated by equaling the mass of the outflow to the mass of the shocked CNM.

A denser CNM (i.e. a higher A) would produce a brighter and earlier radio flare, since the energy transformed to the shock is the same. Figure 4 shows that the peak luminosities span a wide range from  $10^{34}$  erg/s to  $10^{40}$  erg/s. It suggests that the radiation properties are much more sensitive to the outflow velocity, because an order-of-magnitude decrease in velocity causes a greater (six order-of-magnitude) change in luminosity.

#### 4. APPLICATION

In this section, we apply our model to five TDE candidates with late-time radio flares: AT2018hyz, AT2019azh, ASASSN-15oi, IGR J12580+0134 and AT2020vwl. Their radio light curves are shown in Figure 5, with peak luminosities of  $10^{37} \sim 10^{39}$  erg/s.

These TDEs are divided into two groups: one with prompt radio flare and one without. The prompt radio flare here refers to a flare that peaks within about 100 days after the TDEs, such as AT2019azh and AT2020vwl, or the temporal evolution of the flux is slow and relatively smooth, consistent with the prediction of the outflow-CNM scenario, such as IGRJ12580+0134. The other group, which includes ASASSN-15oi and AT2018hyz, instead shows late, sharply rising radio flares, while the early observations give upper limits only.

Here, we attribute the prompt radio flare to the interaction of the outflow with the CNM, while the late-time radio flare is from the interaction of the slightly decelerated, but still fast outflow with the cloud. For

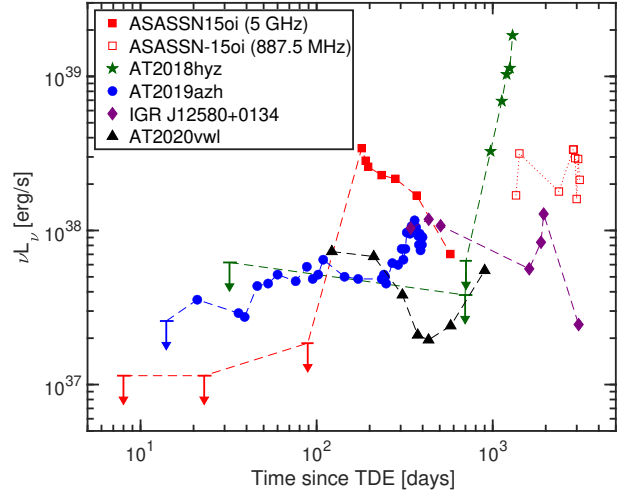


**Figure 5.** Light curves of tidal disruption events with late-time radio flare: ASASSN-15oi(5 GHz, Horesh et al. (2021); 887.5 MHz Anumarlapudi et al. (2024), the observed frequency by VLASS at 1,414 and 2,376 days is about 3 GHz, and the displayed data is the transformed results by  $f_{887.5 \text{ MHz}} = f_{3 \text{ GHz}} [887.5 \text{ MHz}/3 \text{ GHz}]^{1/3}$ ), AT2018hyz (5 GHz, Cendes et al. (2022)), AT2019azh (5.5 GHz, Sfaradi et al. (2022)), IGR J12580+0134 (1.5 GHz, Perlman et al. (2022)) and AT2020vwl (5.5 GHz, Goodwin et al. (2023)), including early upper limits.

ASASSN-15oi and AT2018hyz, we argue that the CNM is dilute, so that the prompt flares are missing.

##### 4.1. AT2020vwl

Figure 6 shows the model fittings of the temporal evolution of the spectra from the outflow-CNM interaction for AT2020vwl with parameters listed in Table 1. The peak frequency from observations exhibits a slow decay that our model can reproduce, and the spectrum at 577 days is well explained by the outflow-CNM interaction for which we consider it may not be related to the outflow-cloud interaction.

Figure 7 shows the light curves comparison at 5GHz. Due to lack of observation, here the green dashed line is to demonstrate that the interaction of the outflow with the cloud is capable of generating this bright late-time radio flare after 600 days.

##### 4.2. AT2019azh

Similar to AT2020vwl, the 15.5 GHz radio observation in AT2019azh shows an early rise of about 30 days and is followed by a late-time brighter radio flare with a peak luminosity of  $10^{38}$  erg/s (Sfaradi et al. 2022). Figure 8 shows the light curves from the model calculation, compared with the observational data at 15.5 GHz. The parameters adopted are listed in Table 1.

**Table 1.** Parameters for the outflow-cloud interaction model applied to the late radio flares in five TDEs, as well as those for the outflow-CNM interactions applied to the simultaneous radio flare. The multiple flares in ASASSN-15oi require five clouds (see Figure 12).

	CNM	Forward shock			Outflow		Cloud		Bow shock	
	$A$ [ $10^3 \text{ cm}^{-3}$ ]	$\epsilon_e$ [ $10^{-2}$ ]	$\epsilon_b$ [ $10^{-3}$ ]	$v_w$ [ $c$ ]	$m_w$ [ $10^{-2} M_\odot$ ]	$t_w$ [ $10^2 \text{ day}$ ]	$R_{in}$ [ $10^{-1} \text{ pc}$ ]	$R_c$ [ $10^{-1} \text{ pc}$ ]	$\epsilon_e$ [ $10^{-2}$ ]	$\epsilon_b$ [ $10^{-3}$ ]
AT 2020vwl	5.8	2	1	0.24	0.6	0.4	1.22	0.81	20	100
AT 2019azh	1.4	1	2	0.36	0.4	1.2	0.75	0.34	8	10
IGR J12580+0134	7	1	1	0.41	4	0.56	4.23	1.9	10	100
AT 2018hyz				0.8	17	3.12	5.6	2.13	5	1
ASASSN-15oi(1)				0.85	1	0.3	0.66	0.1	5	1
ASASSN-15oi(2)				0.8			1.13	0.3	2	2
ASASSN-15oi(3)				0.73			1.52	0.67	2	3
ASASSN-15oi(4)				0.70			6.67	1.75	20	100
ASASSN-15oi(5)				0.68			12.4	4.3	20	100

Interaction of the outflow with the CNM produces a radio flare that peaks at about 100 days. Later when the cloud is hit by the decelerating but high-speed outflow, a late-time radio flare is generated. The power-law index of the temporal decay of the outflow mass rate  $\dot{m}(t', r)$  determines how fast the flare decays and we found an index of 3 is preferred over 5/3. Without spectra observations, the parameters are one example of those with reasonable values and there is degeneracy among them.

#### 4.3. IGR J12580+0134

The radio emission of IGR J12580+0134 was detected 350 days after the X-ray outburst and shows a decline, while later observation at 1,300 days reveals a second flare in the radio with a peak luminosity of  $10^{38}$  erg/s (Perlman et al. 2022). Figure 9 shows the comparison of our model with the observed data at different frequencies. The parameters adopted are listed in Table 1.

For the interaction of the outflow with the CNM, frequencies higher than the  $\nu_a$  would all peak at  $t_{dec}$ , while lower frequencies would peak at a later time when  $\nu_a$  crosses them. As for the interaction of the decelerating outflow with the cloud, the predicted light curves are expected to peak at the same time  $t' = t_w$  since these observational frequencies are all higher than  $\nu_a$  in our model.

#### 4.4. AT2018hyz

The late-time radio flare in AT2018hyz appeared almost 1000 days after the optical discovery with a luminosity of  $10^{39}$  erg/s (Gomez et al. 2020; Cendes et al. 2022).

Figure 10 shows the comparison between the observed radio light curve and the model prediction, while Figure 11 shows the modeling of the spectra. The steep rise of

the flare is well reproduced by the outflow-cloud model. The model also shows a rapid decay after the peak of the flare, if there is no other outflow-cloud interaction.

#### 4.5. ASASSN-15oi

Significant radio detection of ASASSN-15oi began after about 190 days with a flux of 1.3 mJy and showed a decline after. A rebrightening at 3 GHz with a flux of 8.4 mJy is detected approximately 1,400 days after the optical discovery (Horesh et al. 2021). Recently, Australian SKA Pathfinder (ASKAP) observations reveal flux variations after  $t = 2,000$  days (Anumarlapudi et al. 2024).

ASASSN-15oi is the only candidate having multiple late-time radio flares, thus in our model additional clouds are needed. As for the flare before 700 days, apart from the sudden change of the peak frequency at the 4th observation, the complex evolution of the light curve (fast - slow - fast decay) is not predicted by our model (see Figure 5). We suspect the flare before 1000 days comes from the interaction of the outflow with at least two closely located clouds. Overall, we consider these multiple late-time radio flares are from the interaction of the outflow with at least five giant clouds at different distances. Figure 12 shows the modeling of the light curve and Figure 13 shows the spectra comparison. The adapted parameter values for these five collisions are shown in Table 1.

Here among these collisions, the total mass of the outflow remains unchanged. The radial width  $t_w(r)$  increases with distance due to the radial expansion of the outflow. The adapted value of the outflow velocity  $v_w$  decreases after each cloud collision due to the dissipation of the kinetic energy and in addition due to the sweeping of the CNM. In addition, as the outflow moves outwards

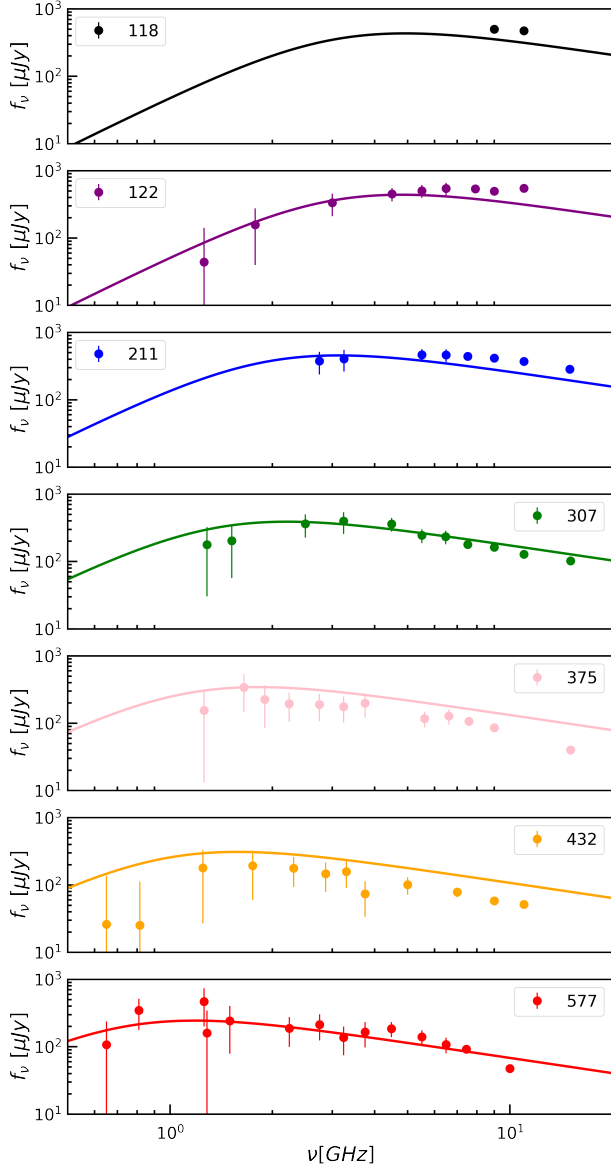


**Figure 6.** Model fittings of the temporal evolution of the spectra from the outflow-CNM interaction for AT2020vwl.

and the density of the outflow decreases, we found that the adopted  $\epsilon_e$  and  $\epsilon_b$  for the last two clouds have to be much greater than the inner clouds to account for the later brighter flares.

## 5. DISCUSSION

Here we discuss an off-axis jet, which can produce the steep rise as observed and is proposed to be one of the explanations for these late radio flares (Matsumoto & Piran 2023; Sfaradi et al. 2024). Also, we would analyze the effect of the density distribution of CNM on the prompt radio flare, and an accompanying possible X-ray emission from the outflow-cloud interaction.

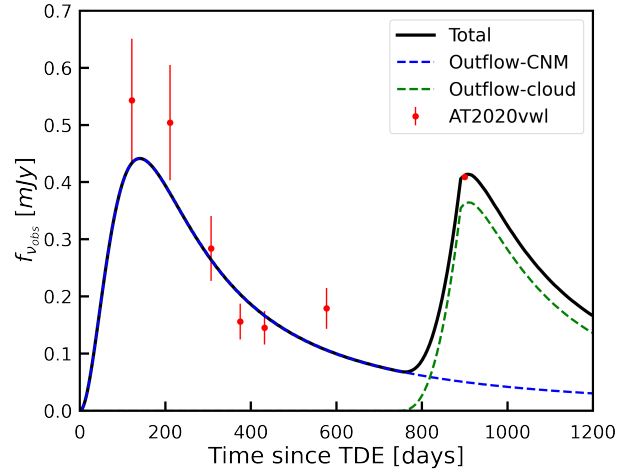


**Figure 7.** Comparison of the model calculation with observation for AT2020vwl at 5GHz. Here we consider the emission from the outflow-CNM interaction (blue dashed line), and that from the outflow-cloud interaction (green dashed line). The combined flux is shown in the black solid line.

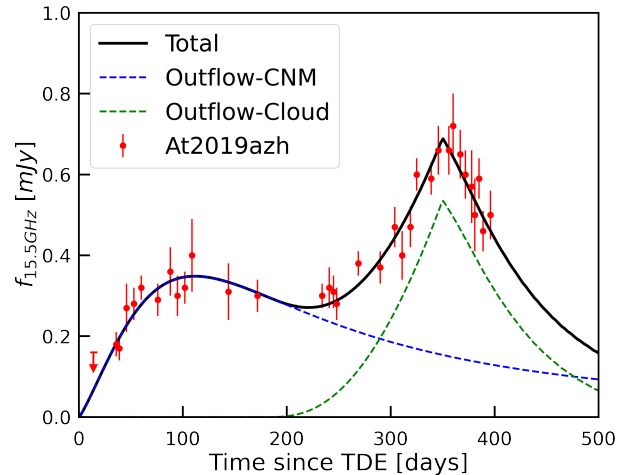


**Figure 8.** Same as Figure 7 but for AT2019azh at 15.5 GHz, including early upper limit.

### 5.1. An off-axis jet

A TDE might generate a relativistic jet (Frank & Rees 1976; De Colle et al. 2012; Metzger et al. 2012). The shock interaction between the relativistic jet and the CNM powers non-thermal radio synchrotron radiation (Giannios & Metzger 2011). The radio signal is beamed away from the observers initially if we are not located within the initial jet aperture  $\theta_j$  (an off-axis jet). As the jet decelerates, the emission from the jet becomes detectable to observers at larger viewing angles  $\theta_{obs}$ , producing a steep rise as  $f_\nu \propto t^{(15-3p)/2}$  for  $\nu > \max(\nu_m, \nu_a)$  (Rhoads 1999; Granot et al. 2002).



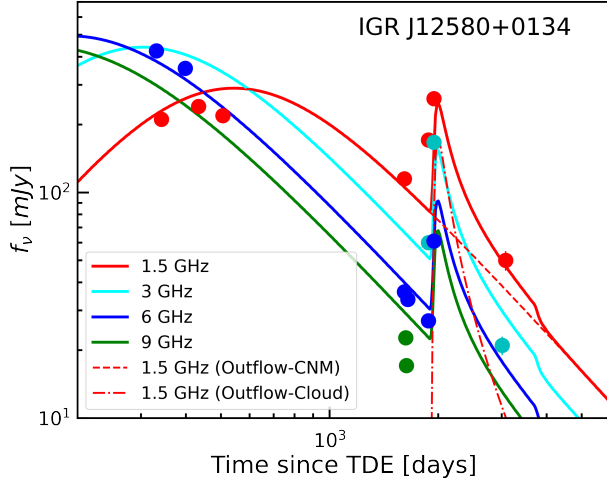


**Figure 9.** Same as Figure 7 for IGRJ12580+0134 at different frequencies.

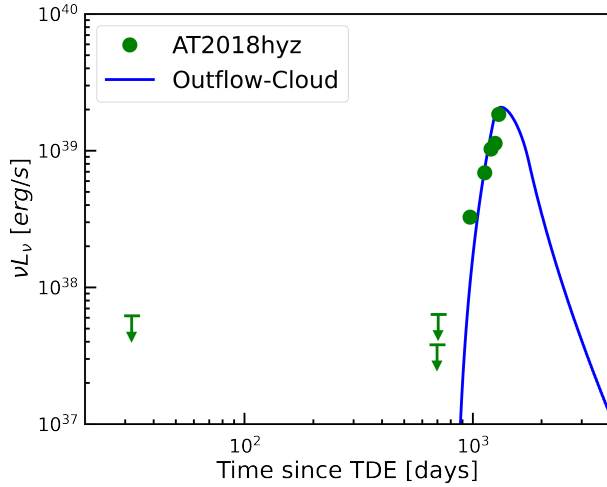


**Figure 10.** Comparison of the model calculation with observation for AT2018hyz at 5 GHz, including early upper limits. Here the outflow-CNM interaction is not considered, since radio emission is not detected at  $t < 10^3$  days.

In the off-axis jet scenario, the radio would peak at the time  $t_p$  with a peak luminosity  $\nu L_\nu$  ( $\nu = 1$  GHz) as (Nakar et al. 2002; Gottlieb et al. 2019):

$$t_p = 60 n_0^{-1/3} E_{52}^{1/3} \left( \frac{\theta_{obs} - \theta_j}{15^\circ} \right)^2 [\text{day}] \quad (15)$$

$$\nu L_\nu \approx 1.1 \times 10^{38} \epsilon_{e,-1}^{p-1} \epsilon_{b,-3}^{(p+1)/4} n_0^{(p+1)/4} E_{52} \left( \frac{\theta_{obs}}{20^\circ} \right)^{-2p} [\text{erg/s}] \quad (16)$$

where  $E_{52}$  is the energy of the jet in units of  $10^{52}$  erg;  $n_0$  is the uniform ambient density in  $\text{cm}^{-3}$ . The equations reveal that a flare with a peak time of about 1,000 days and a peak luminosity of  $10^{39}$  erg/s is possible.

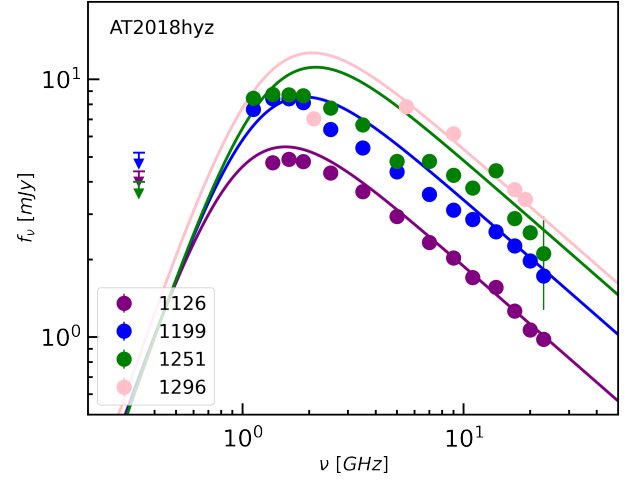


**Figure 11.** Model fittings of the temporal evolution of the spectra from the outflow-cloud interaction for AT2018hyz, including early upper limits.

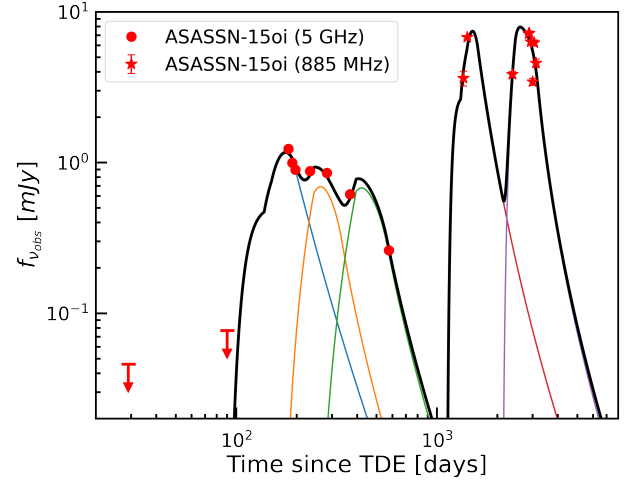


**Figure 12.** The modeling of radio light curves at 5 GHz and 885 MHz for ASASSN-15oi, including early upper limits. The emission is from the interaction of the outflow with five giant clouds at different distances. The different color thin lines mark the light curve from different clouds while the thick black line marks the total light curve. The parameters adopted are listed in Table 1.

Sfaradi et al. (2024) find that the off-axis jet model can explain the full set of radio observations of AT2018hyz. However, the delayed radio flare seen in ASASSN-15oi cannot be explained by such a model, as Horesh et al. (2021) find that its best-fit parameters vary substantially between each epoch and no numerical solution can account for both the initial steep flux rise, and the complex spectral and temporal evolution. Sato et al. (2024) find that a structured two-component jet (a relativistic inner component and trans-relativistic outer component), instead of the one-component jet, can explain the

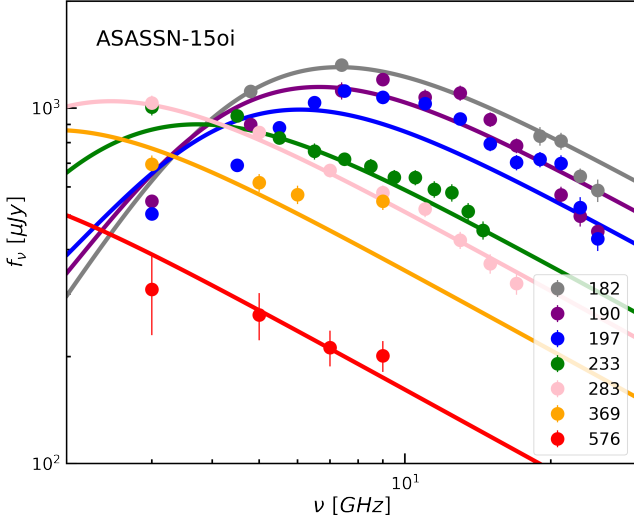


**Figure 13.** Model fittings of the temporal evolution of the spectra from the outflow-clouds interaction for ASASSN-15oi.

radio data of ASASSN-15oi before 1,400 days, as well as ASASSN-1eae, AT2018hyz and AT2019dsg. Nevertheless, the latest observed flux variation after 1,400 days in ASASSN-15oi is unlikely to be explained by this model.

### 5.2. The impact of CNM

The appearance of the prompt radio flare is determined by the density of the CNM. For ASASSN-15oi and AT2018hyz without the prompt radio flare, a dilute CNM is expected. Considering an outflow mass of  $0.01 M_{\odot}$ , a cloud distance of 0.1 pc, and a CNM number density profile the same as the Milky Way as  $n_{CNM} = 3 \times 10^2 r_{-2}^{-1} \text{ cm}^{-3}$  (Xu et al. 2006; Gillessen et al. 2019), the total mass compassed within  $R_{in}$  is  $0.005 M_{\odot}$ . This suggests that the outflow would not decelerate before colliding with the cloud and a bright late-time radio flare is expected. So the Milky Way-like CNM is expected for ASASSN-15oi and AT2018hyz.

For AT2019azh, AT2020vwl and IGR J12580+0134 with the prompt radio flare, a dense CNM is expected, so that a radio flare from the interaction of the outflow with CNM is produced. However, the CNM should not be too dense, otherwise, the velocity of the outflow would have decreased significantly before colliding with the cloud, leading to a dim and undetectable late-time radio flare.

Moreover, an excessively dense CNM has a risk of collapsing onto the galaxy center if the cooling timescale of the CNM  $t_{cool}$  is much shorter than the dynamical timescale  $t_{dyn} = r/v_{ff}$  where  $v_{ff} \sim 100 \text{ km/s}$  is the free-fall velocity of the CNM (White & Rees 1978; Gan et al. 2019). According to the virial theorem, the temperature of the CNM is  $T = m_p v_{ff}^2 / 2k = 10^6 (v_{ff} / 167 \text{ km/s}) \text{ K}$

(Kereš et al. 2005). The cooling timescale is  $t_{cool} = \frac{3}{2} \rho k T / n^2 \Lambda(T)$  (Blondin et al. 1998) where  $\Lambda(T)$  is the temperature-dependent volume cooling function (Raymond et al. 1976; Blondin et al. 1998) and can be reduced as  $\Lambda(T) \approx 6 \times 10^{-27} T^{1/2} \text{ [erg cm}^3/\text{s]}$  (Lin & Murray 2000) for  $v_{ff} \sim 100 \text{ km/s}$  where the dominant radiative cooling mechanisms are bremsstrahlung and recombination processes (Dalgarno & McCray 1972). The necessary collapse condition,  $t_{cool} \leq t_{dyn}$ , is satisfied when the density of the CNM exceeds the critical value  $n_{cri} \approx 2 \times 10^4 r_{-2}^{-1} T_6 \text{ cm}^{-3}$  where  $T_6 \equiv T / 10^6 \text{ K}$ .

Therefore, a mildly dense CNM ( $n_{CNM} \sim 10^3 r_{-2}^{-1} \text{ cm}^{-3}$ ) without a risk of collapsing is adopted for those events with the prompt radio flare.

### 5.3. X-ray emission from the outflow-clouds interaction

The interaction of outflow with a cloud can also drive a cloud shock that propagates into the cloud (McKee & Cowie 1975). The velocity of the cloud shock is:

$$\begin{aligned} \beta_{sc} &= \beta_w \chi^{-1/2} \\ &= 3.8 \times 10^{-3} \beta_{w,-1}^{1/2} \Omega_w^{-1/2} \dot{m}_{w,-1}^{1/2} n_{c,7}^{-1/2} r_{-1}^{-1}, \end{aligned} \quad (17)$$

Where  $\chi = n_c/n_w \sim 10^3$  is the density ratio;  $n_{c,7} = n_c / 10^7 \text{ cm}^{-3}$  is the gas number density of the cloud. The velocity of the bow shock is greater than that of the cloud shock, so the radio emission would be dominated by the shocked outflow. The temperature of the shocked cloud material is :

$$\begin{aligned} T_{sc} &= \frac{3m_H v_{sc}^2}{16k} \\ &= 3 \times 10^7 \beta_{w,-1} \Omega_w^{-1} \dot{m}_{w,-1} n_{c,7}^{-1} r_{-1}^{-2} \text{ [K]}, \end{aligned} \quad (18)$$

which means that the shocked cloud radiates in X-rays.

The internal energy gained by the shocked cloud per unit time is  $E_{c,th} = \frac{9}{32} \rho_c r^2 v_{sc}^3 \Omega_c$ , and the energy conversion efficiency is :

$$\begin{aligned} \eta &= \frac{E_{c,th}}{L_w} \\ &= 0.58 \frac{\Omega_c}{\Omega_w} \chi^{-1/2} \\ &= 2.1\% \beta_{w,-1}^{-1/2} \Omega_w^{-3/2} \dot{m}_{w,-1}^{1/2} n_{c,7}^{-1/2} r_{-1}^{-1}, \end{aligned} \quad (19)$$

where the  $L_w$  is the kinetic luminosity of the outflow. Given that the inferred total energy of the outflow is about  $E_w \sim 10^{50 \sim 51} \text{ erg}$ , then the energy gained by the cloud is  $E_{sc} \sim 10^{48 \sim 49} \text{ erg}$ .

Assuming that the total energy gained by the shocked cloud will be lost by radiative cooling, and substituting Eq.(18) into the cooling timescale formula (see Section

5.1), we have:

$$t_{cool} = 8.7 \times 10^6 \beta_{w,-1}^{1/2} \Omega_w^{-1/2} \dot{m}_{w,-1}^{1/2} n_{c,7}^{-3/2} r_{-1}^{-1} \text{ [s]}. \quad (20)$$

Then the X-ray luminosity from the shocked cloud can be estimated as:

$$\begin{aligned} L_X &\approx \frac{\eta E_w}{t_{cool}} \\ &\approx 2.5 \times 10^{41} E_{w,50} \Omega_w^{-1} \Omega_c \beta_{w,-1}^{-1} n_{c,7} \text{ [erg/s]}, \quad (21) \end{aligned}$$

where  $E_{w,50} \equiv E_w/10^{50}$  erg, both  $\Omega_w$  and  $\Omega_c$  are about unity. This result agrees with the prediction of the X-ray luminosity from the outflow-cloud interaction by [Mou et al. \(2021\)](#) and [Zhuang & Shen \(2021\)](#).

It is clear from Eq.(18) and (19) that when the density ratio  $\chi$  is higher, the shocked cloud is inefficient in generating X-ray radiation. In addition, the optical depth, which is dominated by the Thomson scattering, of the shocked cloud plasma  $\tau \approx n_{c,7} R_{c,-1}$  would increase as well. On the other hand, when  $\chi$  is smaller, the cooling timescale would increase as  $t_{cool} \propto n_c^{-2}$  approximately. Combined with Eq.(19), we have  $L_X \propto n_c^{3/2}$  which shows that the estimated X-ray luminosity would be lower accordingly. As a result, the late-time radio flares may not be accompanied by a late-time X-ray flare.

In addition, [Chen & Wang \(2023\)](#) found that the thermal conduction inside the cloud can play a crucial role in increasing the cloud's radiation, and up to 5~10% of the kinetic energy of the outflow impacting cloud could be converted into radiation. In this case, the estimated luminosity would become  $L_X = \eta E_w/t_{cool} \approx 1.2 \times 10^{43} \eta \beta_{w,-1}^{-1/2} \Omega_w^{1/2} \dot{m}_{w,-1}^{-1/2} n_{c,7}^{3/2} r_{-1}^{-1}$  erg/s ( $\eta = 5 \sim 10\% \Omega_c/\Omega_w$ ).

## 6. CONCLUSION

In recent years, radio observation of some TDEs reveals flares only at a late time ( $10^2 \sim 10^3$  days after TDE discovery), such as in ASASSN-15oi and AT2018hyz, both of which have a radio luminosity of about  $10^{39}$  erg/s. Due to the rapid evolution of light curves, some of these late-time radio flares are difficult to be explained by the conventional outflow-CNM interaction, of which the steepest evolution is  $f_\nu \propto t^3$  ([Metzger et al. 2012](#); [Krolik et al. 2016](#); [Alexander et al. 2020](#)) while observation requires a temporal power-law steeper than  $t^4$ .

A variety of explanations have been proposed for these late-time radio flares such as a delayed launch of the outflow ([Cendes et al. 2023](#)), a misaligned precessing jets ([Lu et al. 2023](#)), an off-axis jet ([Matsumoto & Piran](#)

[2023](#); [Sfaradi et al. 2024](#)), and a piecewise power-law distribution of CNM ([Matsumoto & Piran 2024](#)).

In this paper, we developed a model for the late-time radio flares in which they are produced by the interaction of the outflow with the circum-nuclear gaseous clouds. This collision forms a bow shock, and the late-time radio synchrotron emission is produced from the shocked outflow. We found it is capable of generating bright radio flares years after TDE with a luminosity of  $10^{39}$  erg/s.

The model is applied to five TDE candidates and our model can well explain the observed data, including the multiple late-time flares such as seen in ASASSN-15oi, when the outflow impacts multiple clouds. The inferred outflow velocity ranges from  $0.2c$  to  $0.9c$  with a mass outflow rate of about  $0.01 \sim 0.1 M_\odot/\text{year}$ . The corresponding kinetic luminosity of these outflows is about  $10^{44 \sim 45}$  erg/s which is consistent with the simulation ([Strubbe & Quataert 2009](#); [Curd & Narayan 2019](#); [Bu et al. 2023b,a](#)), and the total kinetic energy of the outflow is  $10^{50} \sim 10^{51}$  erg with a total mass of about  $0.01 \sim 0.1 M_\odot$ . The distances of the cloud ( $\sim 0.1$  pc) are compatible with observations ([Mezger et al. 1996](#); [Christopher et al. 2005](#); [Armijos-Abendaño et al. 2022](#)).

Note that although our model can explain the large delay, the sharpness of the rise and the multiplicity of the late radio flares, the adopted parameter values are not unique and there are degeneracies among them. Therefore, these values cannot be regarded as being exclusively constrained.

Our model may be tested by the accompanied X-ray or dust echo emission component. [Chen & Wang \(2023\)](#) suggested that the late-time X-ray emissions in ASASSN-15oi and AT2019azh can be explained by the outflow-cloud collision, which indicates this interaction may play an important role in the afterglow of TDEs. In addition, there may be lots of dust in the torus as well, such that high-energy emission from TDEs accretion such as X-ray may be absorbed and reprocessed into the infrared ([Lu et al. 2016](#)).

With more late-time radio flares by future observation, we will examine whether our model can be applied to these events and offer constraints on the outflow to help better understand TDEs. In addition, they can also be used as a tool to study the circumnuclear environment.

## ACKNOWLEDGEMENTS

This work is supported by National Natural Science Foundation of China (grants 12073091 and 12261141691) and by the Strategic Priority Research Program of Chinese Academy of Sciences (grant XDB0550200). G.M. is supported by the NSFC (No.12133007).

## REFERENCES

- Alexander, K. D., Berger, E., Guillochon, J., Zauderer, B. A., & Williams, P. K. G. 2016, *ApJL*, 819, L25, doi: [10.3847/2041-8205/819/2/L25](https://doi.org/10.3847/2041-8205/819/2/L25)
- Alexander, K. D., van Velzen, S., Horesh, A., & Zauderer, B. A. 2020, *SSRv*, 216, 81, doi: [10.1007/s11214-020-00702-w](https://doi.org/10.1007/s11214-020-00702-w)
- Antonucci, R. 1993, *ARA&A*, 31, 473, doi: [10.1146/annurev.aa.31.090193.002353](https://doi.org/10.1146/annurev.aa.31.090193.002353)
- Anumarlapudi, A., Kaplan, D., Dobie, D., et al. 2024, *The Astronomer's Telegram*, 16502, 1
- Armijos-Abendaño, J., López, E., Llerena, M., & Logan, C. H. A. 2022, *MNRAS*, 514, 1535, doi: [10.1093/mnras/stac1442](https://doi.org/10.1093/mnras/stac1442)
- Barkov, M. V., Lyutikov, M., & Khangulyan, D. 2019, *MNRAS*, 484, 4760, doi: [10.1093/mnras/stz213](https://doi.org/10.1093/mnras/stz213)
- Barniol Duran, R., Nakar, E., & Piran, T. 2013, *ApJ*, 772, 78, doi: [10.1088/0004-637X/772/1/78](https://doi.org/10.1088/0004-637X/772/1/78)
- Beniamini, P., Nava, L., & Piran, T. 2016, *MNRAS*, 461, 51, doi: [10.1093/mnras/stw1331](https://doi.org/10.1093/mnras/stw1331)
- Blandford, R. D., & Znajek, R. L. 1977, *MNRAS*, 179, 433, doi: [10.1093/mnras/179.3.433](https://doi.org/10.1093/mnras/179.3.433)
- Blondin, J. M., Wright, E. B., Borkowski, K. J., & Reynolds, S. P. 1998, *ApJ*, 500, 342, doi: [10.1086/305708](https://doi.org/10.1086/305708)
- Bloom, J. S., Giannios, D., Metzger, B. D., et al. 2011, *Science*, 333, 203, doi: [10.1126/science.1207150](https://doi.org/10.1126/science.1207150)
- Bu, D.-F., Chen, L., Mou, G., Qiao, E., & Yang, X.-H. 2023a, *MNRAS*, 521, 4180, doi: [10.1093/mnras/stad804](https://doi.org/10.1093/mnras/stad804)
- Bu, D.-F., Qiao, E., & Yang, X.-H. 2023b, *MNRAS*, 523, 4136, doi: [10.1093/mnras/stad1696](https://doi.org/10.1093/mnras/stad1696)
- Burrows, D. N., Kennea, J. A., Ghisellini, G., et al. 2011, *Nature*, 476, 421, doi: [10.1038/nature10374](https://doi.org/10.1038/nature10374)
- Cendes, Y., Alexander, K. D., Berger, E., et al. 2021, *ApJ*, 919, 127, doi: [10.3847/1538-4357/ac110a](https://doi.org/10.3847/1538-4357/ac110a)
- Cendes, Y., Berger, E., Alexander, K. D., et al. 2022, *ApJ*, 938, 28, doi: [10.3847/1538-4357/ac88d0](https://doi.org/10.3847/1538-4357/ac88d0)
- . 2023, arXiv e-prints, arXiv:2308.13595, doi: [10.48550/arXiv.2308.13595](https://doi.org/10.48550/arXiv.2308.13595)
- Chen, J., & Wang, W. 2023, *MNRAS*, 518, 5163, doi: [10.1093/mnras/stac3409](https://doi.org/10.1093/mnras/stac3409)
- Chevalier, R. A. 1998, *ApJ*, 499, 810, doi: [10.1086/305676](https://doi.org/10.1086/305676)
- Christopher, M. H., Scoville, N. Z., Stolovy, S. R., & Yun, M. S. 2005, *ApJ*, 622, 346, doi: [10.1086/427911](https://doi.org/10.1086/427911)
- Coppejans, D. L., Margutti, R., Terreran, G., et al. 2020, *ApJL*, 895, L23, doi: [10.3847/2041-8213/ab8cc7](https://doi.org/10.3847/2041-8213/ab8cc7)
- Curd, B., & Narayan, R. 2019, *MNRAS*, 483, 565, doi: [10.1093/mnras/sty3134](https://doi.org/10.1093/mnras/sty3134)
- Dai, L., McKinney, J. C., Roth, N., Ramirez-Ruiz, E., & Miller, M. C. 2018, *ApJL*, 859, L20, doi: [10.3847/2041-8213/aab429](https://doi.org/10.3847/2041-8213/aab429)
- Dai, Z. G., Huang, Y. F., & Lu, T. 1999, *ApJ*, 520, 634, doi: [10.1086/307463](https://doi.org/10.1086/307463)
- Dalgarno, A., & McCray, R. A. 1972, *ARA&A*, 10, 375, doi: [10.1146/annurev.aa.10.090172.002111](https://doi.org/10.1146/annurev.aa.10.090172.002111)
- De Colle, F., Guillochon, J., Naiman, J., & Ramirez-Ruiz, E. 2012, *ApJ*, 760, 103, doi: [10.1088/0004-637X/760/2/103](https://doi.org/10.1088/0004-637X/760/2/103)
- Ferrarese, L., & Ford, H. 2005, *SSRv*, 116, 523, doi: [10.1007/s11214-005-3947-6](https://doi.org/10.1007/s11214-005-3947-6)
- Frank, J., & Rees, M. J. 1976, *MNRAS*, 176, 633, doi: [10.1093/mnras/176.3.633](https://doi.org/10.1093/mnras/176.3.633)
- Gaisser, T. K., Protheroe, R. J., & Stanev, T. 1998, *ApJ*, 492, 219, doi: [10.1086/305011](https://doi.org/10.1086/305011)
- Gan, Z., Ciotti, L., Ostriker, J. P., & Yuan, F. 2019, *ApJ*, 872, 167, doi: [10.3847/1538-4357/ab0206](https://doi.org/10.3847/1538-4357/ab0206)
- Gao, H., Lei, W.-H., Wu, X.-F., & Zhang, B. 2013, *MNRAS*, 435, 2520, doi: [10.1093/mnras/stt1461](https://doi.org/10.1093/mnras/stt1461)
- Giannios, D., & Metzger, B. D. 2011, *MNRAS*, 416, 2102, doi: [10.1111/j.1365-2966.2011.19188.x](https://doi.org/10.1111/j.1365-2966.2011.19188.x)
- Gillessen, S., Plewa, P. M., Widmann, F., et al. 2019, *ApJ*, 871, 126, doi: [10.3847/1538-4357/aaf4f8](https://doi.org/10.3847/1538-4357/aaf4f8)
- Gomez, S., Nicholl, M., Short, P., et al. 2020, *MNRAS*, 497, 1925, doi: [10.1093/mnras/staa2099](https://doi.org/10.1093/mnras/staa2099)
- Goodwin, A. J., Alexander, K. D., Miller-Jones, J. C. A., et al. 2023, *MNRAS*, doi: [10.1093/mnras/stad1258](https://doi.org/10.1093/mnras/stad1258)
- Gottlieb, O., Nakar, E., & Piran, T. 2019, *MNRAS*, 488, 2405, doi: [10.1093/mnras/stz1906](https://doi.org/10.1093/mnras/stz1906)
- Granot, J., Panaitescu, A., Kumar, P., & Woosley, S. E. 2002, *ApJL*, 570, L61, doi: [10.1086/340991](https://doi.org/10.1086/340991)
- Granot, J., & Sari, R. 2002, *ApJ*, 568, 820, doi: [10.1086/338966](https://doi.org/10.1086/338966)
- Granot, J., & van der Horst, A. J. 2014, *PASA*, 31, e008, doi: [10.1017/pasa.2013.44](https://doi.org/10.1017/pasa.2013.44)
- Guillochon, J., McCourt, M., Chen, X., Johnson, M. D., & Berger, E. 2016, *ApJ*, 822, 48, doi: [10.3847/0004-637X/822/1/48](https://doi.org/10.3847/0004-637X/822/1/48)
- Guolo, M., Gezari, S., Yao, Y., et al. 2023, arXiv e-prints, arXiv:2308.13019, doi: [10.48550/arXiv.2308.13019](https://doi.org/10.48550/arXiv.2308.13019)
- Horesh, A., Cenko, S. B., & Arcavi, I. 2021, *Nature Astronomy*, 5, 491, doi: [10.1038/s41550-021-01300-8](https://doi.org/10.1038/s41550-021-01300-8)
- Huang, Y. F., Gou, L. J., Dai, Z. G., & Lu, T. 2000, *ApJ*, 543, 90, doi: [10.1086/317076](https://doi.org/10.1086/317076)
- Kereš, D., Katz, N., Weinberg, D. H., & Davé, R. 2005, *MNRAS*, 363, 2, doi: [10.1111/j.1365-2966.2005.09451.x](https://doi.org/10.1111/j.1365-2966.2005.09451.x)
- Krolik, J., Piran, T., Svirski, G., & Cheng, R. M. 2016, *ApJ*, 827, 127, doi: [10.3847/0004-637X/827/2/127](https://doi.org/10.3847/0004-637X/827/2/127)
- Krolik, J. H., & Begelman, M. C. 1988, *ApJ*, 329, 702, doi: [10.1086/166414](https://doi.org/10.1086/166414)

- Lin, D. N. C., & Murray, S. D. 2000, *ApJ*, 540, 170, doi: [10.1086/309317](https://doi.org/10.1086/309317)
- Lu, W., & Bonnerot, C. 2020, *MNRAS*, 492, 686, doi: [10.1093/mnras/stz3405](https://doi.org/10.1093/mnras/stz3405)
- Lu, W., Kumar, P., & Evans, N. J. 2016, *MNRAS*, 458, 575, doi: [10.1093/mnras/stw307](https://doi.org/10.1093/mnras/stw307)
- Lu, W., Matsumoto, T., & Matzner, C. D. 2023, arXiv e-prints, arXiv:2310.15336, doi: [10.48550/arXiv.2310.15336](https://doi.org/10.48550/arXiv.2310.15336)
- Matsumoto, T., & Piran, T. 2023, *MNRAS*, 522, 4565, doi: [10.1093/mnras/stad1269](https://doi.org/10.1093/mnras/stad1269)
- . 2024, arXiv e-prints, arXiv:2404.15966, doi: [10.48550/arXiv.2404.15966](https://doi.org/10.48550/arXiv.2404.15966)
- McKee, C. F., & Cowie, L. L. 1975, *ApJ*, 195, 715, doi: [10.1086/153373](https://doi.org/10.1086/153373)
- Metzger, B. D., Giannios, D., & Mimica, P. 2012, *MNRAS*, 420, 3528, doi: [10.1111/j.1365-2966.2011.20273.x](https://doi.org/10.1111/j.1365-2966.2011.20273.x)
- Mezger, P. G., Duschl, W. J., & Zylka, R. 1996, *A&A Rv*, 7, 289, doi: [10.1007/s001590050007](https://doi.org/10.1007/s001590050007)
- Mou, G., Wang, T., Wang, W., & Yang, J. 2022, *MNRAS*, 510, 3650, doi: [10.1093/mnras/stab3742](https://doi.org/10.1093/mnras/stab3742)
- Mou, G., & Wang, W. 2021, *MNRAS*, 507, 1684, doi: [10.1093/mnras/stab2261](https://doi.org/10.1093/mnras/stab2261)
- Mou, G., Dou, L., Jiang, N., et al. 2021, *ApJ*, 908, 197, doi: [10.3847/1538-4357/abd475](https://doi.org/10.3847/1538-4357/abd475)
- Nakar, E., Piran, T., & Granot, J. 2002, *ApJ*, 579, 699, doi: [10.1086/342791](https://doi.org/10.1086/342791)
- Perlman, E. S., Meyer, E. T., Wang, Q. D., et al. 2022, *ApJ*, 925, 143, doi: [10.3847/1538-4357/ac3bba](https://doi.org/10.3847/1538-4357/ac3bba)
- Phinney, E. S. 1989, in *The Center of the Galaxy*, ed. M. Morris, Vol. 136, 543
- Raymond, J. C., Cox, D. P., & Smith, B. W. 1976, *ApJ*, 204, 290, doi: [10.1086/154170](https://doi.org/10.1086/154170)
- Rees, M. J. 1988, *Nature*, 333, 523, doi: [10.1038/333523a0](https://doi.org/10.1038/333523a0)
- Rhoads, J. E. 1999, *ApJ*, 525, 737, doi: [10.1086/307907](https://doi.org/10.1086/307907)
- Rybicki, G. B., & Lightman, A. P. 1986, *Radiative Processes in Astrophysics*
- Santana, R., Barniol Duran, R., & Kumar, P. 2014, *ApJ*, 785, 29, doi: [10.1088/0004-637X/785/1/29](https://doi.org/10.1088/0004-637X/785/1/29)
- Sari, R., Piran, T., & Narayan, R. 1998, *ApJL*, 497, L17, doi: [10.1086/311269](https://doi.org/10.1086/311269)
- Sato, Y., Murase, K., Bhattacharya, M., et al. 2024, arXiv e-prints, arXiv:2404.13326, doi: [10.48550/arXiv.2404.13326](https://doi.org/10.48550/arXiv.2404.13326)
- Sfaradi, I., Horesh, A., Fender, R., et al. 2022, *ApJ*, 933, 176, doi: [10.3847/1538-4357/ac74bc](https://doi.org/10.3847/1538-4357/ac74bc)
- Sfaradi, I., Beniamini, P., Horesh, A., et al. 2024, *MNRAS*, 527, 7672, doi: [10.1093/mnras/stad3717](https://doi.org/10.1093/mnras/stad3717)
- Strubbe, L. E., & Quataert, E. 2009, *MNRAS*, 400, 2070, doi: [10.1111/j.1365-2966.2009.15599.x](https://doi.org/10.1111/j.1365-2966.2009.15599.x)
- Sturmer, S. J., Skibo, J. G., Dermer, C. D., & Mattox, J. R. 1997, *ApJ*, 490, 619, doi: [10.1086/304894](https://doi.org/10.1086/304894)
- Tchekhovskoy, A., Narayan, R., & McKinney, J. C. 2011, *MNRAS*, 418, L79, doi: [10.1111/j.1745-3933.2011.01147.x](https://doi.org/10.1111/j.1745-3933.2011.01147.x)
- Teboul, O., & Metzger, B. D. 2023, *ApJL*, 957, L9, doi: [10.3847/2041-8213/ad0037](https://doi.org/10.3847/2041-8213/ad0037)
- White, S. D. M., & Rees, M. J. 1978, *MNRAS*, 183, 341, doi: [10.1093/mnras/183.3.341](https://doi.org/10.1093/mnras/183.3.341)
- Wu, H.-J., Mou, G., Wang, K., Wang, W., & Li, Z. 2022, *MNRAS*, 514, 4406, doi: [10.1093/mnras/stac1621](https://doi.org/10.1093/mnras/stac1621)
- Xu, Y.-D., Narayan, R., Quataert, E., Yuan, F., & Baganoff, F. K. 2006, *ApJ*, 640, 319, doi: [10.1086/499932](https://doi.org/10.1086/499932)
- Yalinewich, A., Steinberg, E., Piran, T., & Krolik, J. H. 2019, *MNRAS*, 487, 4083, doi: [10.1093/mnras/stz1567](https://doi.org/10.1093/mnras/stz1567)
- Zhang, B.-B., van Eerten, H., Burrows, D. N., et al. 2015, *ApJ*, 806, 15, doi: [10.1088/0004-637X/806/1/15](https://doi.org/10.1088/0004-637X/806/1/15)
- Zhuang, J., & Shen, R.-F. 2021, *Journal of High Energy Astrophysics*, 32, 11, doi: [10.1016/j.jheap.2021.06.001](https://doi.org/10.1016/j.jheap.2021.06.001)